The modelling of carbon-based supercapacitors: distributions of time constants and Pascal Equivalent Circuits

Journal of Power Sources 345 (2017) 247–253

Contents lists available at ScienceDirect

Journal of Power Sources

journal homepage: www.elsevier.com/locate/jpowsour

The modelling of carbon-based supercapacitors: Distributions of time constants and Pascal Equivalent Circuits

Stephen Fletcher [a, *], Iain Kirkpatrick [a], Roderick Dring [a], Robert Puttock [a], Rob Thring [b], Simon Howroyd [b]

[a] Department of Chemistry, Loughborough University, Leicestershire, LE11 3TU, UK
[b] Department of Aeronautical and Automotive Engineering, Loughborough University, Leicestershire, LE11 3TU, UK

HIGHLIGHTS

- Two probability models of supercapacitor electrodes are developed.
- Wide distributions of resistance and capacitance are considered.
- "Pascal Equivalent Circuits" explain many puzzling phenomena.
- Non-exponential responses are due to continuous distributions of *RC* time constants.

GRAPHICAL ABSTRACT

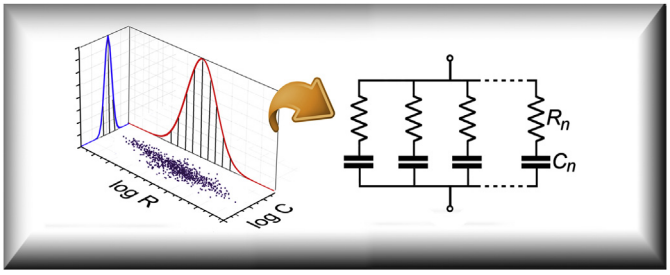

ARTICLE INFO

Article history:
Received 5 October 2016
Received in revised form
4 January 2017
Accepted 4 February 2017
Available online 11 February 2017

Keywords:
Supercapacitor
Carbon electrode
Pascal Equivalent Circuit
Voltage rebound
Simscape
MATLAB

ABSTRACT

Supercapacitors are an emerging technology with applications in pulse power, motive power, and energy storage. However, their carbon electrodes show a variety of non-ideal behaviours that have so far eluded explanation. These include *Voltage Decay* after charging, *Voltage Rebound* after discharging, and *Dispersed Kinetics* at long times. In the present work, we establish that a vertical ladder network of *RC* components can reproduce all these puzzling phenomena. Both software and hardware realizations of the network are described.

In general, porous carbon electrodes contain random distributions of resistance *R* and capacitance *C*, with a wider spread of log *R* values than log *C* values. To understand what this implies, a simplified model is developed in which log *R* is treated as a Gaussian random variable while log *C* is treated as a constant. From this model, a new family of equivalent circuits is developed in which the continuous distribution of log *R* values is replaced by a discrete set of log *R* values drawn from a geometric series. We call these *Pascal Equivalent Circuits*. Their behaviour is shown to resemble closely that of real supercapacitors. The results confirm that distributions of *RC* time constants dominate the behaviour of real supercapacitors.

1. Introduction

Recently, a *Universal Equivalent Circuit* was proposed for carbon-based supercapacitors [1]. For a single carbon electrode (or two matched carbon electrodes in one cell) the circuit consists of a vertical ladder network of *RC* components, with each "rung" of the ladder having its own characteristic time constant, see Fig. 1. In the

* Corresponding author.
E-mail addresses: S.Fletcher2@lboro.ac.uk (S. Fletcher), I.Kirkpatrick@lboro.ac.uk (I. Kirkpatrick), R.A.Dring2@lboro.ac.uk (R. Dring), robb.puttock@gmail.com (R. Puttock), R.H.Thring@lboro.ac.uk (R. Thring), S.Howroyd@lboro.ac.uk (S. Howroyd).

http://dx.doi.org/10.1016/j.jpowsour.2017.02.012

present work, we develop software and hardware realizations of this model, and then compare their responses with real supercapacitors.

Supercapacitors differ from ideal capacitors in a number of important ways. For example, they show voltage decay at open circuit, capacitance loss at high frequency, and voltammetric distortions at high scan rate. Why do these phenomena occur? The short answer is that the complex network of pores inside activated carbon behaves like a vast collection of micro-capacitors wired in parallel, with each wire having its own resistance. As a result, supercapacitors exhibit *asynchronous charging*. That is, each micro-capacitor charges at a different rate. The existence of this phenomenon explains why "mean field" models of carbon electrodes (which assume that all pores charge at the same rate) fail to capture the full transient dynamics of real systems.

Although there are many ways of parameterizing the ladder network shown in Fig. 1A, the most natural choice is to use the admittance y, because admittances in parallel are additive. We therefore adopt that approach here. To begin, we focus on the n th rung of the ladder network considered in isolation. In that case, the parameters R_n and C_n are constants and the individual rung admittance (siemens) is given by the equation

$$y_{\mathrm{n}}(\omega) = \frac{j\omega C_{\mathrm{n}}}{1 + j\omega R_{\mathrm{n}} C_{\mathrm{n}}} \tag{1}$$

where the ranges of R_{n} and C_{n} are assumed to be strictly positive. Evidently, the time constant of each rung is $R_{\mathrm{n}}C_{\mathrm{n}} = \tau_{\mathrm{n}}$.

Now we consider all the rungs in parallel. The total admittance of the ladder Y_{L} is obtained by performing the summation

$$Y_{\mathrm{L}}(\omega) = \sum_{n=1}^{N_L} y_{\mathrm{n}} \tag{2}$$

where N_L (dimensionless) is the total number of rungs in the ladder, and R_{n} and C_{n} are discrete random variables. For a few hundred rungs having known values of R_{n} and C_{n} this sum can be computed term-by-term. However, for millions of rungs having broad distributions of R_{n} and C_{n} the evaluation of Y_{L} is more challenging.

To make progress, we assume that the population of rungs in the ladder is so dense that the distributions of R_{n} and C_{n} are effectively continuous. We also assume that the distributions of R_{n} and C_{n} are statistically independent. In that case we can define a joint probability density function $\theta(R, C)$ having a single normalization

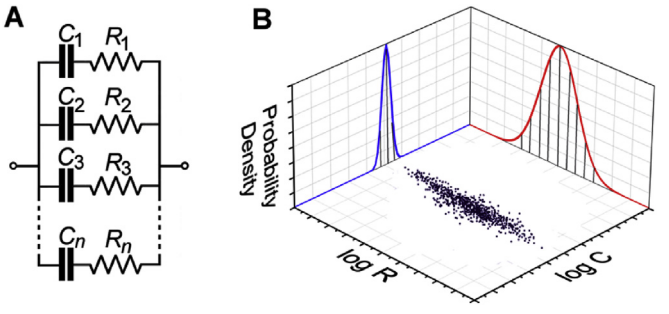

Fig. 1. A. Equivalent circuit of a supercapacitor electrode. Each "rung" has its own characteristic RC time constant. B. Idealized diagram of the joint distribution of log R and log C values inside an activated carbon electrode. One point on the plane corresponds to one rung on the ladder network. Note that there is a much wider spread of log R values than log C values.

$$\int_0^\infty \int_0^\infty \theta(R, C) dR\, dC = 1 \tag{3}$$

This then allows us to write Eq. (2) in the compact form

$$Y_{\mathrm{L}}(\omega) = N_{\mathrm{L}} \int_0^\infty \int_0^\infty \frac{j\omega C}{1 + j\omega RC} \theta(R, C) dR\, dC \tag{4}$$

where the ranges of R and C are again assumed to be strictly positive.

Ideally, we should like to measure $\theta(R, C)$ directly. However, in the absence of experimental techniques for doing this, we here develop some useful approximations of Eq. (4) valid in cases where the range of either R or C is severely restricted. The first model that we consider (denoted Model I) assumes that the micro-capacitors are all different while the resistors are all the same. The second model (denoted Model II) assumes that the resistors are all different while the capacitors are all the same.

1.1. Derivation of Model I

If C is a random variable while R is a constant, then the total admittance Y_{L} of the ladder network as a function of frequency ω takes the much simpler form:

$$Y_{\mathrm{L}}(\omega) = Y_{\mathrm{L}}(\infty) \int_0^\infty \frac{j\omega\tau}{1 + j\omega\tau} g(\tau) d\tau \tag{5}$$

Or equivalently

$$Y_{\mathrm{L}}(\omega) = \frac{N_{\mathrm{L}}}{R} \int_0^\infty \frac{j\omega\tau}{1 + j\omega\tau} g(\tau) d\tau \tag{6}$$

Here R is the resistance of one rung in the ladder, N_{L} is the total number of rungs in the ladder, and $g(\tau)$ is the normalized probability density function of τ, i.e. the spectrum of RC time constants in the system:

$$\int_0^\infty g(\tau) d\tau = 1 \tag{7}$$

In the case of a lumped equivalent circuit, the function $g(\tau)$ will have a finite number of discrete "spectral lines" corresponding to the finite number of RC time constants. In the case of a real electrode, however, the function $g(\tau)$ will be essentially continuous.

1.2. Derivation of Model II

If R is a random variable while C is a constant, then the total admittance Y_{L} of the ladder network as a function of frequency ω takes the form:

$$Y_{\mathrm{L}}(\omega) = Y_{\mathrm{L}}(0) \int_0^\infty \frac{f(\tau)}{1 + j\omega\tau} d\tau \tag{8}$$

Or equivalently

$$Y_{\mathrm{L}}(\omega) = j\omega C N_{\mathrm{L}} \int_0^\infty \frac{f(\tau)}{1 + j\omega\tau} d\tau \tag{9}$$

Here C is the capacitance of one rung in the ladder, N_L is the total number of rungs in the ladder, and $f(\tau)$ is the normalized probability density function of τ, i.e. the spectrum of RC time constants in the system:

$$\int_0^\infty f(\tau)d\tau = 1 \tag{10}$$

Model I was developed more than thirty years ago by Brug et al. to quantify inhomogeneous surfaces on uniformly accessible electrodes [2]. Model II, however, is new, and is used here to quantify homogeneous surfaces on non-uniformly accessible electrodes (porous carbon).

Inside porous carbon, the pore radii typically have values over the range $r \approx 0.1$ nm to $r \approx 10.0$ μm, which spans five orders of magnitude. This implies that pore resistances may have values that span *ten* orders of magnitude, since (for cylindrical pores) the pore resistance is given by the formula

$$R_{\text{pore}} = \frac{\rho L}{\pi r^2} \tag{11}$$

Here ρ is the pore resistivity, L is the pore length, and r is the pore radius. By contrast, surface capacitances of carbon typically have values over the range $C = 2$ μF cm^{-2} to $C = 70$ μF cm^{-2}, depending on whether graphitic basal planes or oxidized edge planes are exposed [3]. Such a range of capacitance values spans less than two orders of magnitude. Overall, therefore, Model II appears much closer to reality. An idealized diagram of the joint distribution of $\log R$ and $\log C$ values inside an activated carbon electrode is shown in Fig. 1B.

2. Experimental and results

In order to explore some of the properties of Model II, we now introduce a new family of equivalent circuits that can mimic the wide distributions of resistances found in carbon supercapacitors. We call them “Pascal Equivalent Circuits”. Unlike conventional equivalent circuits, Pascal Equivalent Circuits are not “mean field” approximations, and therefore they are not restricted to a small number of RC time constants. Instead, they have 2^{n-1} RC elements arranged in a vertical ladder network, with a single value of C, but multiple values of R drawn from a geometric series. The number of resistors of a particular value of R is determined by the coefficients of the n^{th} row of Pascal's Triangle (Fig. 2A).

To illustrate the idea, a “Row 5” Pascal Equivalent Circuit is shown in Fig. 2B. This is a 16-rung vertical ladder network having five sets of RC values arranged in sequence of their time constants. Each set of RC values contains a population of “rungs” determined by the binomial coefficients: 1, 4, 6, 4, 1. Consistent with Model II, all the micro-capacitors are the same, but the sets of resistors differ by factors of ten. As a result, the Pascal Equivalent Circuit displays an approximately lognormal distribution of RC time constants (i.e. a normal distribution of $\log \tau$ values), and thus resembles the very broad distribution of RC time constants found in real supercapacitors.

The theoretical link between Pascal's triangle and the lognormal distribution is provided by the binomial distribution. In the notation of Fig. 2A, the binomial distribution takes the form

$$\Pr(X = k) = C(n,k)p^k(1-p)^{n-1-k} \tag{12}$$

where

$$C(n,k) = \frac{(n-1)!}{k!(n-1-k)!} \tag{13}$$

and $\Pr(X = k)$ is the probability that the random variable X takes value k. Thus, for the special case $p = 1/2$, the k coefficients along the n^{th} row of Pascal's triangle are identical to the k coefficients of the binomial distribution. (This may readily be verified by substitution.) Further, by a well-known result in statistics, the binomial distribution approaches the normal distribution for large n; this trend is illustrated in Fig. 2C. [Explicitly, if the distribution of the random variable X is binomial $B(n,p)$ then for sufficiently large n the distribution approaches the normal form $N(\mu,\sigma)$ with $\mu = np$ and $\sigma^2 = np(1-p)$.] Finally, the normal distribution may be transformed into a lognormal distribution by replacing successive values of k with successive values of a geometric series $Y(k)$. For example, when constructing trial models in the present work, we found it convenient to use the decadal values $Y = 10^k$ where $k = 1, 2, 3 \ldots n$.

The probability density function of a lognormally-distributed parameter Y is given by the equation

$$\lambda(Y) = \frac{1}{\sigma Y\sqrt{2\pi}}\exp\left(-\frac{[\ln(Y)-\mu]^2}{2\sigma^2}\right) \tag{14}$$

where μ and σ are the mean and standard deviation of the underlying normal distribution. A plot of $\lambda(Y)$ versus Y is shown in Fig. 2D. Clearly the lognormal density function is strongly skewed to the right, where it is responsible for the very large time constants that appear in practical devices. Interestingly, the skewness is a sensitive function of the underlying standard deviation σ,

$$\text{Skewness} = \left[\exp\left(\sigma^2\right) + 2\right]\sqrt{\exp(\sigma^2) - 1} \tag{15}$$

2.1. Voltage decay at open circuit

One feature of real supercapacitors that Pascal Equivalent Circuits reproduce outstandingly well is the phenomenon of *Voltage Decay* at open circuit. An example is shown in Fig. 3A. This illustrates the effect of charging the “Row 5” Pascal Equivalent Circuit shown in Fig. 2B for different periods of time at 2.0 V. Upon switching to open circuit, the fast-responding micro-capacitors (i.e. those that have completed their charging process at 2.0 V) immediately begin to discharge into the slow-responding micro-capacitors (i.e. those that have not completed their charging process at 2.0 V), thus causing the *Voltage Decay*.

From a health and safety perspective, it is reassuring to note that the *Voltage Decay* in real supercapacitors is not due to uncontrolled electrochemical reactions inside the carbon electrodes. Instead, it is due to the wide distribution of RC time constants in the pores, and can therefore be avoided simply by charging devices for longer times. (Even the most resistive pores will become charged eventually, even if it takes 24 h).

2.2. Voltage rebound

Traditionally, it has been difficult to simulate large electrical circuits such as the one illustrated in Fig. 2B. However, equivalent circuit modelling has recently become much easier with the release of Simscape™, a high-level programming language developed by MathWorks, Inc. (Natick, Massachusetts, USA) [4]. Simscape™ not only allows researchers to model electrical equivalent circuits of arbitrary size, but also allows the models to be run on a digital

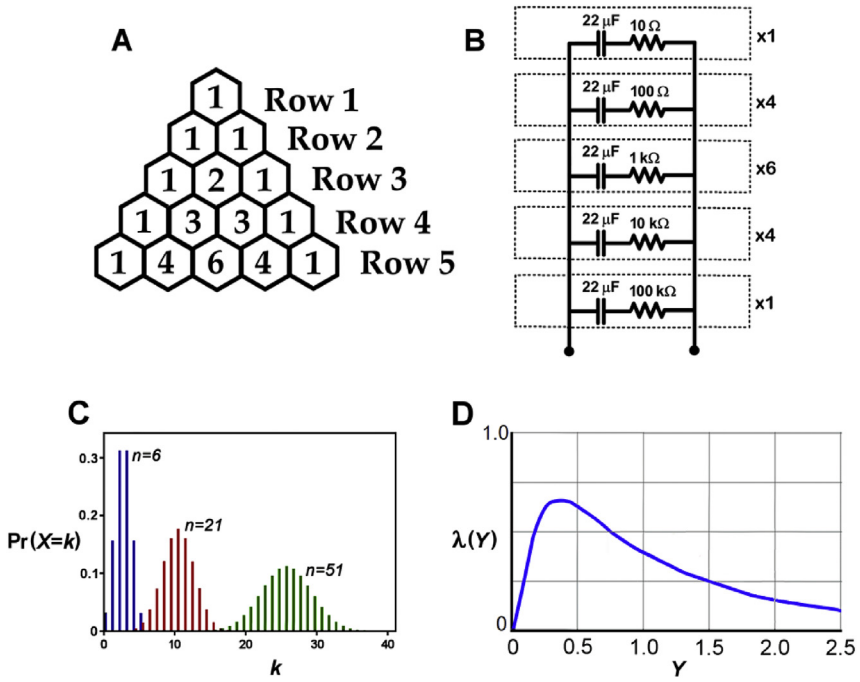

Fig. 2. A. Binomial Coefficients of Pascal's Triangle, showing the numbering system used in the present work. B. A "Row 5" Pascal Equivalent Circuit. Each "rung" of the ladder consists of a capacitor and a resistor in series. In this example, the capacitors all have value 22 μF whereas the sets of resistors differ by factors of ten between 10 Ω and 100 kΩ. The smallest *RC* time constant is 220 μs and the largest time constant is 2.2 s. In between these limiting cases the resulting distribution of time constants is approximately lognormal. C. Graphical representation of the coefficients of Pascal's triangle for selected values of *n*. The probabilities $\Pr(X = k)$ are identical to the coefficients of Pascal's triangle divided by $2n - 1$, and they are also identical to the values of the probability density function of the binomial distribution for the special case $p = 1/2$. D. The probability density function of the lognormal distribution, for the case $\sigma = 1$, $\mu = 0$. Note the extreme skewness to the right.

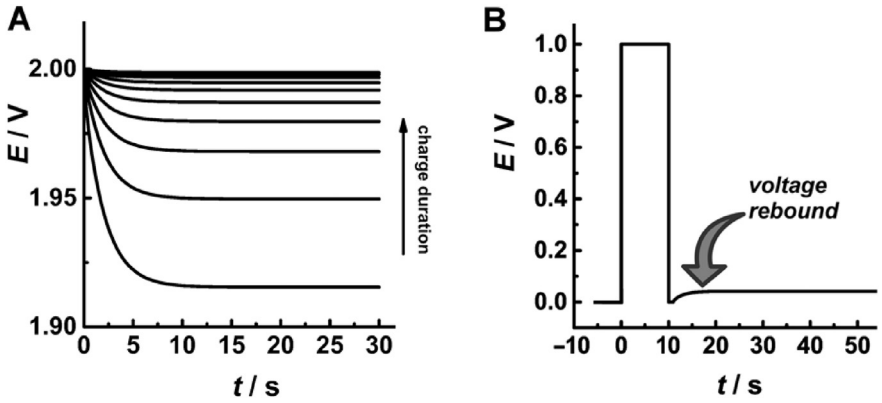

Fig. 3. A. Simscape™ Simulation of a "Row 5" Pascal Equivalent Circuit, showing Voltage Decay at Open Circuit. Plots of open circuit voltage versus time, after charging potentiostatically at 2 V for various durations (1-10 s). B. Simscape™ Simulation of a "Row 5" Pascal Equivalent Circuit, showing Voltage Rebound at Open Circuit. Plot of voltage versus time, after charging potentiostatically at 1 V for 10 *s* and then discharging potentiostatically at 0 V for 1 s. After switching to open circuit, the system exhibits a voltage increases due to the redistribution of charge.

computer. Conveniently, Simscape™ operates in the Simulink® programming environment, and so is fully compatible with MATLAB®.

During the present work, Simscape™ was used to simulate the rapid discharge process of supercapacitors, with the goal of equalizing their terminal voltages and thus rendering them safe. (By definition, a fully discharged supercapacitor at open circuit has a voltage of zero volts.) Some model shut-down data are shown in Fig. 3B. To obtain this plot, a Simscape™ model of the "Row 5" Pascal Equivalent Circuit was charged at 1 V for 10 *s*, and then discharged at 0 V for 1 s. What happened next was very revealing — a *Voltage Rebound* occurred after the system was switched to open circuit.

Analysis of the transient responses of individual "rungs" provided the explanation. On open circuit, the slowest *RC* states (i.e. those which had remained full during the 1 s spent at 0 V) were now re-charging the fastest *RC* states (i.e. those which had emptied during the 1 s spent at 0 V). The spontaneous occurrence of this effect in the Simscape™ model was compelling evidence that it was also occurring in reality. The only remaining question was how broad the distribution of time constants might actually be in a real system.

In theory, a voltage rebound can be generated with as few as two "rungs" in the ladder. However, such a parsimonious allocation of

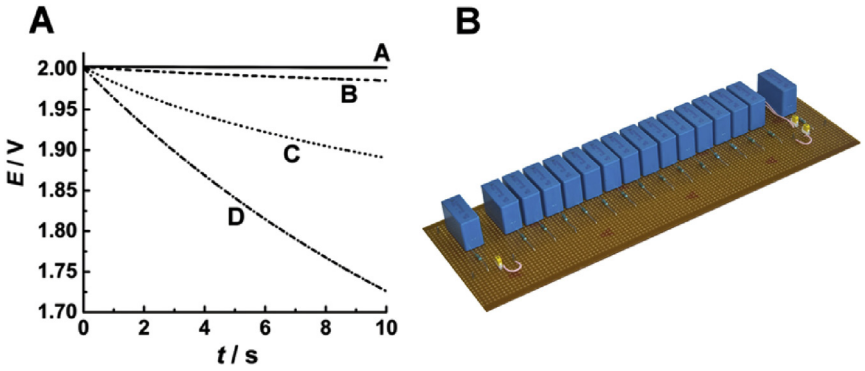

Fig. 4. A. Voltage Decay of commercial capacitors. Plots of voltage versus time for (A) an Epcos aluminium/polyethylene-terephthalate capacitor (solid line), (B) a Panasonic aluminium/aluminium-oxide/conductive-polymer capacitor (dashed line), (C) a Vishay tantalum/tantalum-pentoxide/manganese-dioxide electrolytic capacitor (dotted line), and (D) a Nichicon aluminum/aluminium-oxide electrolytic capacitor (dash-dot line). All data refer to capacitors of 22 μF ±20% charged in series with 1 kΩ resistors at 2 V for 4 s. Note the excellent voltage retention of the aluminium/PET capacitor (top curve). B. Hardware Implementation of a "Row 5" Pascal Equivalent Circuit. The component values are the same as those in Fig. 2B.

time constants is inadequate to model the asymptotic long-time behaviour of real electrodes (see below). In the real world, it turns out that a very broad distribution of time constants is needed.

2.3. *In operando* modelling

The successful implementation of Pascal Equivalent Circuits *in silico* (i.e. as virtual models in a computer) prompted us to explore the possibility of implementing them *in operando* (i.e. as actual physical models in the real world.) Before embarking on this task, however, it was first necessary to ensure that any commercial resistors and capacitors that we used would respond as closely as possible to their mathematically idealized counterparts. It turned out that near-ideal resistors were readily available from many suppliers, but that near-ideal capacitors were not. Indeed, many off-the-shelf capacitors showed voltage decay on the time scale of seconds, which made them useless for our purposes. Some examples of the voltage decay of commercial capacitors are shown in Fig. 4A. Fortunately, the aluminium/polyethylene-terephthalate (PET) capacitors retained their voltage over the timescale of many seconds, so these were used in all our physical models.

In passing, we remark that the physical origin of voltage decay in ordinary capacitors may be different to that in supercapacitors. For example, in ordinary capacitors, voltage decay may be due to current leakage through the dielectric.

By using aluminium/PET capacitors we were able to implement a fully-functioning hardware model of a "Row 5" Pascal Equivalent Circuit on a printed circuit board (Fig. 4B). For ease of comparison, the component values were selected to be the same as those in Fig. 2B. To test the physical device, we recorded plots of its open circuit voltage versus time, after charging potentiostatically at 2 V for various time intervals (1–10 s). The results are shown in Fig. 5A. The similarity of these results with those of the Simscape™ simulation (Fig. 3A) is noteworthy. In both cases, the voltage decay curves are exponential with time constants equal to the largest time constant in the ladder (2.2 s). No slower states are observed.

It is interesting to compare the simulated voltage decay curves with real-world data from a commercial supercapacitor (Fig. 5B). The latter device shows the expected voltage decay, but the voltage-time curves are slightly non-exponential. This is due to the presence of a very long "tail" of ultra-slow states inside the carbon electrodes. The existence of this "tail" means that real supercapacitors must be held at zero volts for 24 h between individual measurements, in order to ensure that their discharge is complete.

In our laboratories, we have found that hardware models of supercapacitors can be very useful for both pedagogical and practical purposes. However, although it is comparatively easy to match the *RC* products of hardware models with those of real supercapacitors, it is sometimes difficult to match the individual values of *R* and *C*. This is because real supercapacitors may have exceptionally high values of *C*. For example, a real supercapacitor may have a capacitance >10 F, much higher than any normal capacitor.

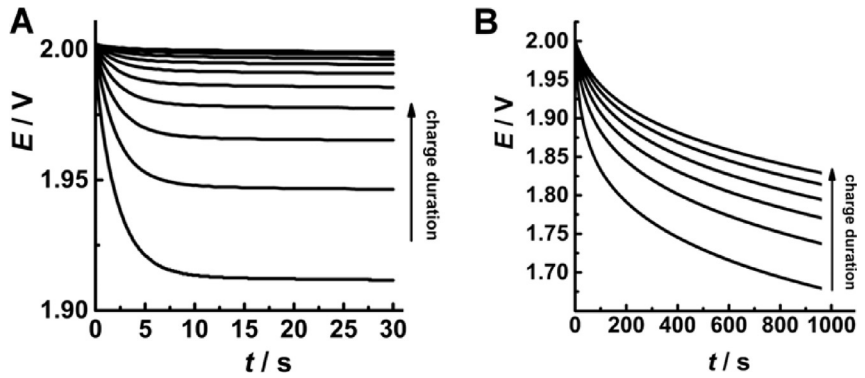

Fig. 5. A. Output of the hardware model of the "Row 5" Pascal Equivalent Circuit, showing Voltage Decay at Open Circuit. Plots of open circuit voltage versus time, after charging potentiostatically at 2 V for various intervals (1–10 s). B. Real-world measurements on an NEC/Tokin activated carbon/sulfuric acid supercapacitor (nominally 10 mF), showing Voltage Decay after charging. Plots of open circuit voltage versus time, after charging potentiostatically at 2 V for various durations (10, 20, 30, 40, 50, 60 s). Terminals short-circuited for 24 h between measurements.

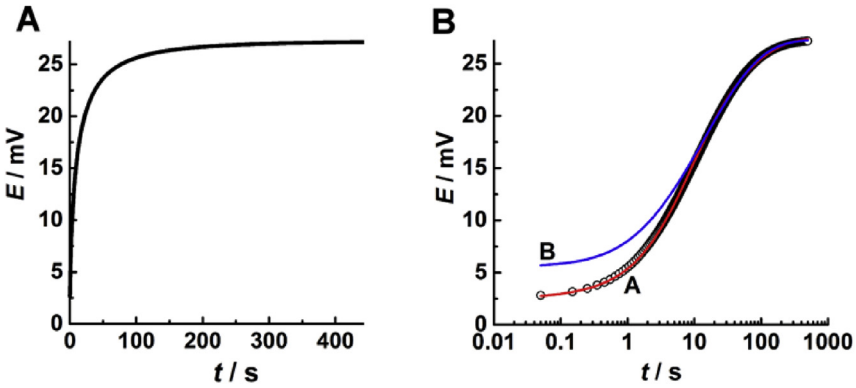

Fig. 6. A. Real-world measurements on an NEC/Tokin activated carbon/sulfuric acid supercapacitor (nominally 10 mF), showing Voltage Rebound after short-circuiting. Open circuit potential versus log (time) for an NEC/Tokin activated carbon/sulfuric acid supercapacitor (nominally 10 mF) after charging at 1 V for 2 s then short-circuiting for 2 s. B. Voltage Rebound (commercial supercapacitor) on a logarithmic time scale. Open circuit potential versus log (time) for an NEC/Tokin activated carbon/sulfuric acid supercapacitor (nominally 10 mF) after charging at 1 V for 2 s then short-circuiting for 2 s. Test of goodness-of-fit of a lognormal distribution of *RC* time constants (A) and for a stretched exponential function (B) with exponent $\beta = 0.6$. Note: data were fitted on a linear timescale, but plotted on a logarithmic time scale.

2.4. Non-exponential voltage decay curves

The *Voltage Decay* curves of real supercapacitors are similar to those of the hardware and software models, except the curve shapes tend to be non-exponential rather than exponential. This subtlety arises from the fact that the *RC* time constants in real supercapacitors are arbitrarily close together, whereas those in the models are a finite distance apart. As a result, real supercapacitors tend to display multi-exponential decays on all time scales. Some typical experimental data are shown in Fig. 5B.

As noted in Section 2.3, powerful evidence for the existence of a distribution of *RC* time constants in real supercapacitors is the appearance of a *Voltage Rebound* after a period at short circuit, coupled with non-exponential voltage-time responses. An example is shown in Fig. 6A. In this case, an NEC/Tokin activated carbon/sulfuric acid supercapacitor (nominally 10 mF) was charged at 1 V for 2 s then short-circuited for 2 s. A rising non-exponential voltage-time curve then appears. This indicates that a re-distribution of electrical charge is taking place from the slower *RC* states to the faster *RC* states inside the carbon electrodes.

In order to curve-fit the voltage-time data we tested two well-known models of dispersed kinetics, namely the stretched exponential model and the lognormal distribution model. The stretched exponential model is obtained by inserting a constant β into the exponential function:

$$f(t) = \exp\Big(-(kt)^{\beta}\Big) \tag{16}$$

Typically, the choice of the constant β is restricted to the range $(0, 1)$ so that a graph of $\log f$ versus t has a "stretched" appearance. Among physicists, the stretched exponential function is also known as the *Kohlrausch function*, after Rudolf Kohlrausch, who used it to model the residual voltage on a Leyden jar [5].

On the other hand, the lognormal distribution model is obtained by inserting the exponential function into a Fredholm integral equation of the first kind:

$$f(t) = \int_0^{\infty} \varphi(k) exp(-kt) \mathrm{d}k \tag{17}$$

where

$$\varphi(k) = \frac{1}{\sigma\sqrt{2\pi}} \exp\left(-\frac{1}{2}\left(\frac{k-\mu}{\sigma}\right)^2\right) \tag{18}$$

Here μ and σ are the mean and standard deviation of the random variable k, and $\varphi(k)$ is its probability density function [6,7]. In other words, the distribution of the argument k is assumed to be normal.

Each of the above models added just one degree of freedom to the classic case of exponential decay. In the case of the stretched exponential function the extra degree of freedom was the exponent β, while in the case of the lognormal distribution the extra degree of freedom was the standard deviation σ. However, in both cases the improvement in the goodness-of-fit was dramatic. Indeed, both distributions could be fitted to the experimental data within experimental error at asymptotically long times, although the lognormal distribution fared slightly better at short times (Fig. 6B). The obvious conclusion is that several theoretical models can be fitted to the experimental data within practical accuracy. That is, the fitting problem is "ill-posed" in the sense of Tikhonov [8].

The experimental observation of smooth, non-exponential, voltage-time plots in real supercapacitors over more than three orders of magnitude in time is powerful evidence in favour of a broad distribution of time constants. If a distribution of time constants is arbitrarily truncated, the models show that the asymptotic behaviour of the voltage at long times is dominated by the largest time constant remaining. Some examples are shown in Fig. 7A and B. These figures provide plots of open circuit voltage versus time for the Simscape™ simulation and for the hardware model, after charging potentiostatically for fixed periods of time. The curves are all exponential functions with time constants of 2.2 s (the slowest in the ladder). No such exponential responses are observed in the real world. Instead, the non-exponential responses indicate the existence of a highly skewed distribution like that in Fig. 2D.

3. Discussion

The vertical ladder network shown in Fig. 1A reproduces many of the characteristic features of carbon-based supercapacitors. However, the exact distribution of *RC* time constants remains an unsolved problem. Clearly, it would be very desirable to measure this distribution with accuracy and precision. At present, however, all we can say is that the distribution is broad and highly skewed to the right.

One method of estimating the distribution of *RC* time constants

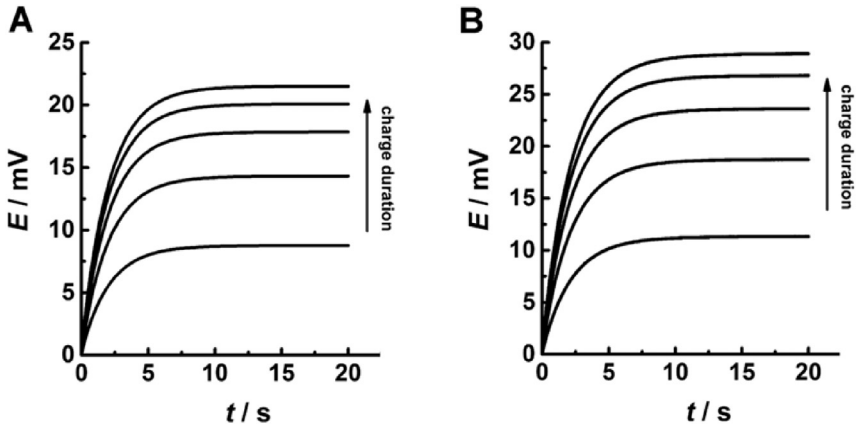

Fig. 7. A Simscape™ Simulation of a "Row 5" Pascal Equivalent Circuit, showing Voltage Rebound. Plots of open circuit voltage versus time, after charging potentiostatically at 1 V for various durations (1-5 s), followed by short circuit for 3 s. The curves are exponential functions with time constants of 2.2 s (the slowest in the ladder). B. Hardware model of a "Row 5" Pascal Equivalent Circuit, showing Voltage Rebound. Plots of open circuit voltage versus time, after charging potentiostatically at 1 V for various durations (1-5 s), followed by short circuit for 3 s. The curves are exponential functions with time constants of 2.2 s (the slowest in the ladder).

is by means of molecular dynamics simulations. As recently shown by Pean et al. [9] these techniques generate molecular level properties that can then be inserted into equivalent circuit models. Similarly, Kondrat and Kornyshev [10] have used Monte Carlo simulations to probe the remarkably complex phenomena that occur inside nanopores. In particular, they have shown how ions and solvent molecules compete for space [11]. In future, it would be instructive to combine these molecular approaches with equivalent circuit theory.

4. Conclusions

In the present work, two probability models of supercapacitor electrodes have been developed based on the assumption that the internal resistance and internal capacitance are random variables. The first model that we considered (denoted Model I) assumed that the capacitance values were widely different, while the resistance values were all the same. The second model that we considered (denoted Model II) assumed that the resistance values were widely different, while the capacitance values were all the same. It was then noted that, in activated carbon electrodes, there was a much wider spread of log R values than log C values, suggesting that Model II was more appropriate.

Model II was then transformed into a new kind of equivalent circuit, which we called a "Pascal Equivalent Circuit". Unlike conventional equivalent circuits, the Pascal Equivalent Circuit was not restricted to a small number of RC time constants, but instead had 2^{n-1} RC elements arranged in a vertical ladder network. The number n could be arbitrarily large. By implementing Pascal Equivalent Circuits in both software and hardware several counter-intuitive responses of supercapacitors were explained. These included *Voltage Decay* after charging, *Voltage Rebound* after discharging, and *Dispersed Kinetics* at long times. All of these were previously mysterious.

Finally, it is interesting to compare the ladder model of Fig. 1A with the literature standard, which is the de Levie transmission line model for a single pore [12–17]. Evidently, the models are mutually indistinguishable (degenerate) if the de Levie model is generalized to many different pores in parallel. The fact that neither model is definitive therefore serves as a warning against over-interpretation of individual resistance and capacitance values derived from one model alone.

Acknowledgements

This work was sponsored by the EPSRC (UK) Grant Number EP/M009394/1, "Electrochemical Vehicle Advanced Technology" (ELEVATE).

References

[1] S. Fletcher, V.J. Black, I. Kirkpatrick, A universal equivalent circuit for carbon-based supercapacitors, J. Solid State Electrochem. 18 (5) (2014) 1377–1387.
[2] G.J. Brug, A.L.G. Van Den Eeden, M. Sluyters-Rehbach, J.H. Sluyters, The analysis of electrode impedances complicated by the presence of a constant phase element, J. Electroanal. Chem. Interfacial Electrochem. 176 (1) (1984) 275–295.
[3] S. Fletcher, Screen-printed carbon electrodes, in: P.N. Bartlett, R.C. Alkire, J. Lipkowski (Eds.), Electrochemistry of Carbon Electrodes, Wiley-VCH, Weinheim, 2015, pp. 419–437.
[4] Anonymous, MatLab, Simulink, Reference Text R2015b, The MathWorks, Inc., 3 Apple Hill Drive, Natick, MA, 2015, 01760–2098.
[5] R. Kohlrausch, Theorie des elektrischen Rückstandes in der Leidener Flasche, Ann. Phys. Chem. 91 (Part I) (1854) 56–82. Part II (179–214).
[6] W. Primak, Kinetics of processes distributed in activation energy, Phys. Rev. 100 (1955) 1677–1689.
[7] W.J. Albery, P.N. Bartlett, C.P. Wilde, J.R. Darwent, A general model for dispersed kinetics in heterogeneous systems, J. Am. Chem. Soc. 107 (7) (1985) 1854–1858.
[8] A.N. Tikhonov, A.V. Goncharsky, V.V. Stepanov, A.G. Yagola, Numerical Methods for the Solution of Ill-posed Problems, vol. 328, Springer Science & Business Media, Dordrecht, 2013.
[9] C. Pean, B. Rotenberg, P. Simon, M. Salanne, Multi-scale modelling of supercapacitors: from molecular simulations to a transmission line model, J. Power Sources 326 (2016) 680–685.
[10] S. Kondrat, A.A. Kornyshev, Pressing a spring: what does it take to maximize the energy storage in nanoporous supercapacitors? Nanoscale Horizons 1 (1) (2016) 45–52.
[11] C.C. Rochester, S. Kondrat, G. Pruessner, A.A. Kornyshev, Charging ultra-nanoporous electrodes with size-asymmetric ions assisted by apolar solvent, J. Phys. Chem. C 120 (2016) 16042–16050.
[12] R. de Levie, On porous electrodes in electrolyte solutions: I. Capacitance effects, Electrochim Acta 8 (1963) 751–780.
[13] R. de Levie, On porous electrodes in electrolyte solutions — IV, Electrochim Acta 9 (1964) 1231–1245.
[14] D.H. Fritts, An analysis of electrochemical capacitors, J. Electrochem Soc. 144 (1997) 2233–2241.
[15] A.M. Johnson, J. Newman, Desalting by means of porous carbon electrodes, J. Electrochem Soc. 118 (1971) 510–517.
[16] F.A. Posey, T. Morozumi, Theory of potentiostatic and galvanostatic charging of the double layer in porous electrodes, J. Electrochem Soc. 113 (1966) 176–184.
[17] S. Fletcher, Contribution to the theory of conducting-polymer electrodes in electrolyte solutions, J. Chem. Soc. Faraday Trans. 89 (1993) 311–320.